BULLETIN OF THE POLISH ACADEMY OF SCIENCES
TECHNICAL SCIENCES
Vol. 57, No. 4, 2009

Power electronic converter for photovoltaic systems with the use of FPGA-based real-time modeling of single phase grid-connected systems

S. PIRÓG*, R. STALA, and Ł. STAWIARSKI

Department of Electrical Drive and Industrial Equipment, AGH University of Science and Technology,
30 Mickiewicza Ave, 30-059 Kraków, Poland

Abstract. The paper presents a method of investigation of grid connected systems with a renewable energy source. The method enables fast prototyping of control systems and power converters components by real-time simulation of the system. Components of the system such as energy source (PV array), converters, filters, sensors and control algorithms are modeled in FPGA IC. Testing the systems before its practical application reduces cost and time-to-market. FPGA devices are commonly used for digital control. The resources of the FPGAs used for preliminary testing can be sufficient for the complete system modelling. Debugging tools for FPGA enable observation of many signals of the analyzed power system (as a result of the control), with very advanced triggering tools. The presented method of simulation with the use of hardware model of the power system in comparison to classical simulation tools gives better possibilities for verification of control algorithms such as MPPT or anti-islanding.

Key words: photovoltaic (PV), FPGA, DSP, digital control, generation of electrical energy, real time simulation, renewable energy systems, power electronic converters.

1. Introduction

The number of photovoltaic-based energy generation systems is fast increasing in the world. There are many advantages of the application of photovoltaic (PV) systems: no cost of energy, no pollution, long lifetime, no rotating parts. New potential fields of application are constantly emerging – e.g. BIPV (Building Integrated Photovoltaic) with solar cells on elastic substrates [1].

PV array is an energy source with the characteristics presented in Fig. 1. Power of PV source depends on the load, irradiance and temperature. The $p(v)$ characteristic of PV panel has one maximum named MPP (Maximum Power Point).

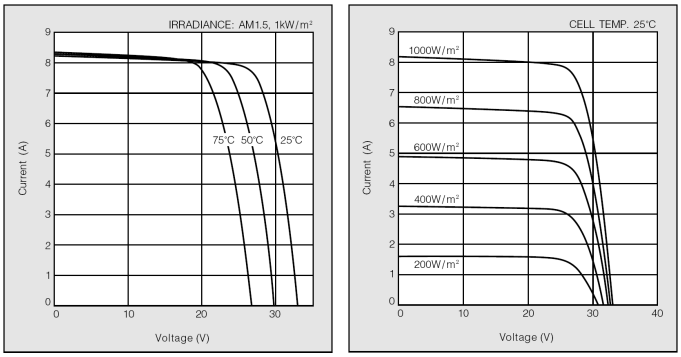

Fig. 1. PV cell characteristics – Kyocera KC200GT Cell after Ref. 6

In most cases of energy generation systems, the PV source operates with power electronic converters [2–3]. The following tasks should be realized by the power electronic conversion stage in PV systems:

- proper load of PV source. Power conversion system forces the PV source to be loaded in its MPP. The algorithm of looking for MPP (MPPT – Maximum Power Point Tracking) makes the PV source best exploited,
- adjusting the energy parameters to the constraints of the customer, e.g. in grid-connected systems the power electronic converters enable generation of current (of proper shape) to the grid, in the island systems the inverter should generate proper voltage.

FPGA (Field Programmable Gate Arrays) chips are commonly used in power electronic control systems. The functional blocks of FPGA, such as logic resources, memory and hardware implemented DSP-type modules [4-6] (Fig. 2), work in parallel using different parts of the FPGA structure.

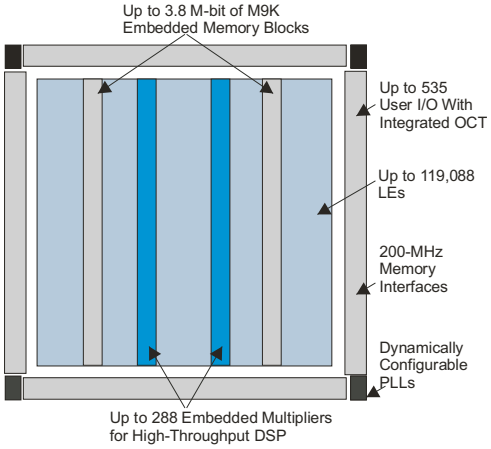

Fig. 2. Altera Cyclone III FPGA resources after Ref. 5

*e-mail: pirog@agh.edu.pl

A single FPGA chip can provide the entire control of complex power electronic systems. Programmability features and CAD-supported design enable shortening time to market by using simulation and debugging tools in design verification. Then, during the application of the control system in industrial systems, the stage of verification of control and protection algorithms on physical process becomes the most difficult, expensive, time-consuming and unsafe stage. The features of FPGAs can help to improve this process by enabling testing the control algorithms on real-time models of controlled systems (Fig. 3).

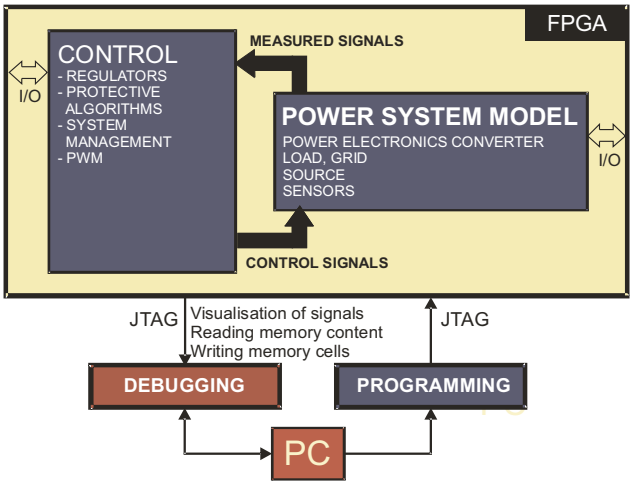

Fig. 3. FPGA (or external DSP) control verification with use of the real-time model

Using a selected FPGA device, the model can be implemented in the same chip as control algorithms. Depending on the application, different topologies of power electronic converters are used in renewable energy generation systems [2–3].

New converters are developed to increase efficiency of power conversion stage, improve its reliability or decrease initial cost. The paper focuses on presenting the method for PV systems testing with the use of real-time simulations in FPGA chip. In [7–9] such method was presented for PV systems components simulation, in [10–11] for multilevel converters simulation, in [12] for the electrical machine modeling, in [13] for induction motor control investigation and in [14] for permanent magnet motor drive simulation. We present results from modeling typical components for single phase PV systems (PV source, dc-dc boost converter, single-phase inverter, ac filters, operation of the grid connected inverter in closed system, regulation of voltage in the boost converter and the MPPT realization).

Photovoltaic systems are highly predisposed to the FPGA prototyping and testing because of their complexity and specific behaviour (e.g. PV source characteristic). Many algorithms of control must cooperate with each other. Apart from the correctness of the control system, operation may be tested under emulated, real operating conditions (e.g. MPPT on PV featured source, grid voltage and impedance, islanding operation, etc.). FPGA-based prototype of the entire PV system may be adequate for the actual system components in details with possibility of making changes. Figure 4 presents two types of single-phase grid-connected systems with PV sources. The paper presents results of investigations of such systems with the use of FPGA-based real-time models.

a)

b)

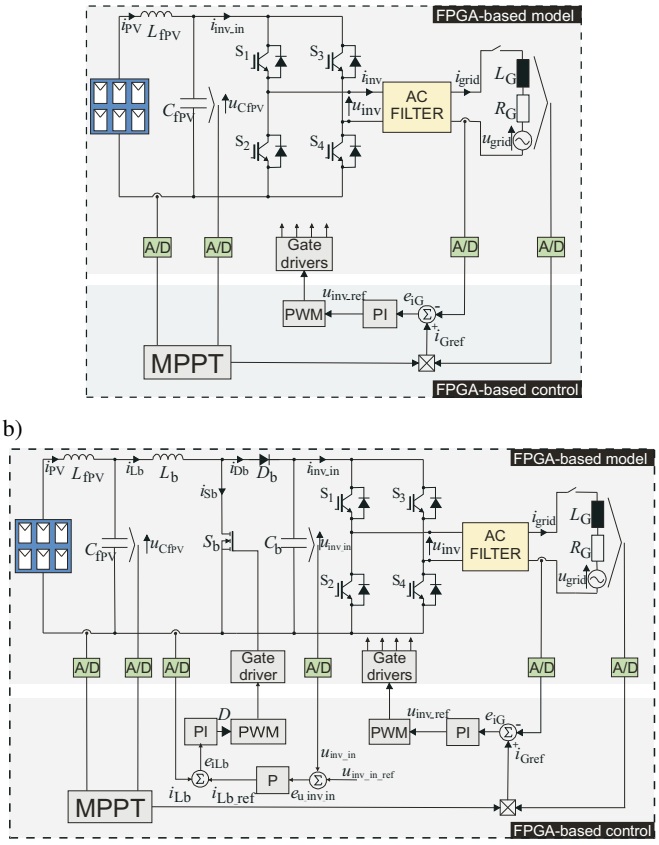

Fig. 4. The analyzed models of single-phase grid-connected systems; a) without and b) with boost converter

In the first system (Fig. 4a) the single phase inverter is supplied directly from the PV source. Such system is commonly used when PV panels voltages are adjusted to the energetic system voltage level (to enable the grid current shaping, and not to exceed the voltage absolute ratings of the system components). In some countries the solar system also needs isolation (e.g. LF transformer in AC filter section, or HF system [2, 3]). The inductor in a solar panel output filter (L_{fPV}) is not always installed but it can decrease the 100 Hz power pulsations in the PV source. The system presented in Fig. 4b is dedicated to be supplied through the PV panels which voltage can decrease below the level that enables proper generation of the grid current by the inverter. The FPGA-based real-time models of the power systems (Fig. 4ab) enable testing the control (MPPT, boost control, inverter control, special control: e.g. start of the system, protection, anti-islanding algorithms implementation) or modification in the topologies (e.g. AC filters topology). The paper focuses on presenting the possibilities of such actions, showing results of models' components behaviour.

In the model tested in this paper, the dc-dc boost converter stabilizes voltage for the inverter on constant level (e.g. 400V). The inverter control unit is responsible for generating the line current to transfer energy to the grid (control loop of inverter – Fig. 4ab) with maximum efficiency of the PV panel (MPPT unit that gives reference grid current amplitude). An example of waveforms from the inverter control unit under steady state operation of the inverter is presented in Fig. 5. The grid voltage and current, the inverter voltage, reference current, error of control and PI-type regulator output signal are presented in Fig. 5. In this case, the shape of reference grid current is acquired by pre-scaling the measured grid voltage. This signal is multiplied by the factor calculated by MPPT unit. Error of the control (e_{iG}) – the difference between reference current (i_{Gref}) and measured current (i_{grid}) passed to PI-type regulator. Output signal of the regulator ($u_{\mathrm{inv\_ref}}$) is a control signal for PWM module. The control system was designed to operate with 50 Hz system.

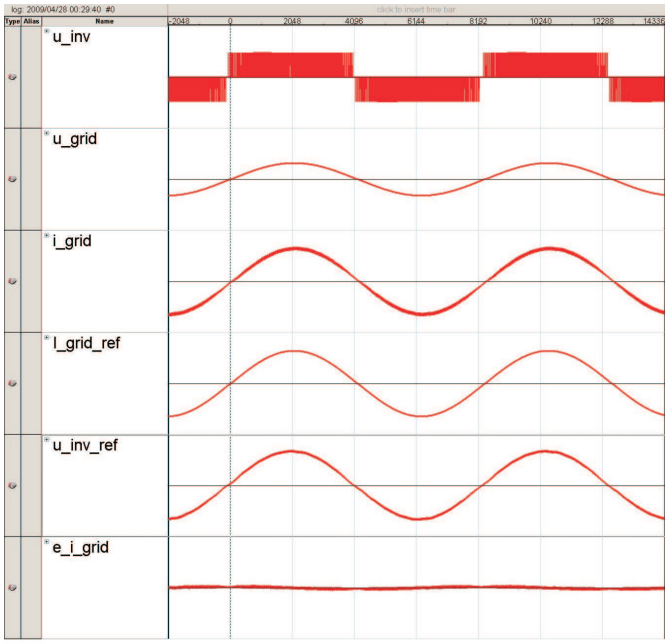

Fig. 5. The control system behavior under steady state operation of the analyzed system (Fig. 4, L-type 2 mH AC filter). Waveforms of grid voltage and current, the inverter voltage, reference current, error of control and PI-type regulator

The model used in this paper has the following parameters:

- Currents and voltages resolution: 18bits
- Controllers calculation step time: $1.33 \cdot 10^{-6}$ s
- Calculation step time for the converters and passive components modelling: $0.2 \cdot 10^{-6}$ s to $0.082 \cdot 10^{-6}$ s

2. FPGA-based model of the PV source

Various methods of simulating PV cell can be found [15-19]. Most of them are based on the diode model of a PV cell. As a result of such modelling, exponential equations which describe $i(u)$ characteristics are given. This approach, despite its good reliability, is difficult to be simply described in VHDL language. In [15] a very suitable model of PV source for FPGA-based discrete modelling is presented. Nonlinear photovoltaic source is represented as a current source with parallel connected resistance which value varies with irradiance and temperature (Fig. 6). Variation of cell resistance is simulated as a switching resistor (Fig. 6).

PV source voltage is described by the following equation (Fig. 6):

$$U_{pv} = R_{eq} \cdot (I_{sc} - I_{pv}) \tag{1}$$

where U_{pv} – PV cell voltage, I_{sc} – PV cell short current – proportional to irradiance level, I_{pv} – PV cell current, R_{eq} – variable equivalent resistor.

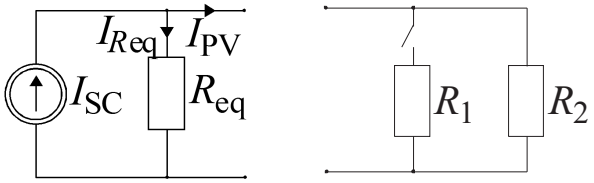

Fig. 6. Model of nonlinear PV source after Ref. 15 and the switching resistance

Equivalent resistance is a parallel connection of the R_2 and switched R_1 resistors (Fig. 6):

$$R_{eq} = \frac{R_1 R_2}{R_1 + R_2 K}. \tag{2}$$

Parameter K is the equivalent of duty cycle D used in [15]. The value of parameter K is computed numerically and $K = 0$ when PV cell is shortened and $K = 1$ under open circuit operation. Thus, K can be defined as:

$$K = 1 - \frac{I_{pv}}{I_{sc}}. \tag{3}$$

In Eqs. (1), (2) and (3) variation in irradiance level is corresponding to proportional change in an open circuit voltage U_{OC} level. But in PV panels the open circuit voltage U_{OC} does not decrease proportionally to the solar irradiation level. To adjust the model, a scaling factor M is implemented to Eq. (2):

$$R_{eq} = \frac{R_1 R_2}{R_1 + R_2 K \cdot M}. \tag{4}$$

The factor M is proportional to the difference between maximum irradiance level ($I_{SC\,\max}$) and decreased irradiance level (I_{SC}) (5).

$$M \approx I_{SC\,\max} - I_{SC}. \tag{5}$$

In order to calculate scaling factor M, the minimal value of R_{eq} for decreased irradiation level ($I_{SC20\%}$) has to be calculated. $R_{eq\,\min}$ parameter is the PV cell resistance under open circuit operation (Fig. 6, $I_{PV} = 0$, $I_{Req} = I_{SC}$). In this paper the PV source model is based on Kyocera KC200GT Cell (Fig. 1) [6]:

$$R_{eq\ \min 20\%} = R_{eq\ \min 100\%} \cdot \frac{U_{OC\ \ 20\%}}{U_{OC\ \ 100\%} \cdot 20\%}. \tag{6}$$

Entering the analyzed PV cell model data:
$R_2 = 120$ [Ω]

$U_{OC\_100\%} = 32.9$ [V] ($E = 1000$ W/m^2, 25°C)
$U_{OC\_20\%} = 30.54$ [V] ($E = 200$ W/m^2, 25°C)
$R_{eq\_\min 100\%} = 4$ [Ω]

The equivalent resistor at 20% of irradiance has following value:

$$R_{eq\_min20\%} = 18.57\ [\Omega]. \tag{7}$$

Changes in $R_{eq\,\min}$ value can be simulated as changes of maximum value of the parameter K (2). For decreased level of irradiation ($I_{SC20\%}$), it can be calculated:

$$K_{\max\_20\%} = 0.188. \tag{8}$$

It means, that for reduced irradiation level ($I_{SC20\%}$), at open circuit operation, value of K must be equal to (8) to provide correct U_{OC} value.

The difference in PV short current values (for irradiation 1000 W/m^2 and 200 W/m^2) is as follows:

$$I_{SC\_100\%} - I_{SC\_20\%} = 8.21 - 1.64 = 6.57\ [\text{A}]. \tag{9}$$

On the basis of the assumption that U_{OC} change is linear (in range of 20%–100% of irradiation), it can be written:

$$\begin{aligned} K_{\max\_20\%} &\Leftrightarrow I_{SC\_100\%} - I_{SC\_20\%}, \\ K_{\max\_100\%} &\Leftrightarrow I_{SC\_100\%} - I_{SC\_100\%} = 0. \end{aligned} \tag{10}$$

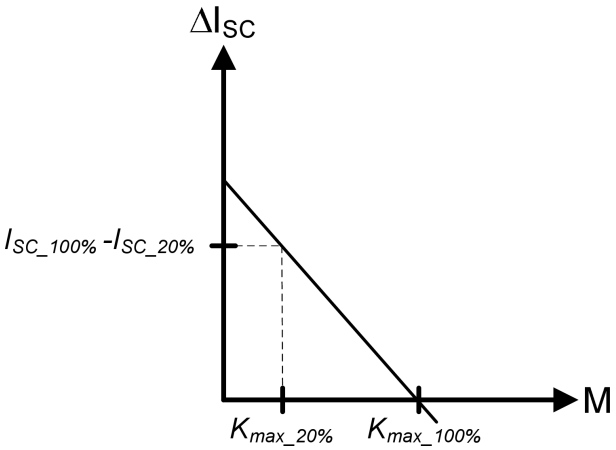

Fig. 7. ΔI_{SC} as a function of scaling factor M (5), (8)

From the Fig. 7 it follows that:

$$\begin{aligned} &I_{SC\_100\%} - I_{SC} = \\ &= \left(\frac{I_{SC\_100\%} - I_{SC\_20\%}}{K_{\max\_20\%}}\right) \cdot M - \left(\frac{I_{SC\_100\%} - I_{SC\_20\%}}{K_{\max\_20\%}}\right). \end{aligned} \tag{11}$$

Value of scaling factor M for analyzed PV cell model:

$$M = 1 - 0.124 \cdot (8.21 - I_{SC})\,. \tag{12}$$

On the basis of (1), (3), (4) and (12), the complete formula for calculating of PV cell voltage can be obtained:

$$U_{PV} = \frac{R_1 R_2 \left(I_{SC} - I_{PV}\right)}{R_1 + R_2 \left(1 - \frac{I_{PV}}{I_{SC}}\right)\left(1 - 0.124\left(I_{SC\_100\%} - I_{SC}\right)\right)}. \tag{13}$$

A very important parameter of a PV cell is the temperature of the semiconductor junction. To implement the temperature influence the PV source model is extended by scaling R_{eq} and $I_{SC\_100\%}$ parameters with temperature T[°C]:

$$\begin{aligned} R_{eq\_T} &= R_{eq\_0^o} - 0.01424 \cdot T, \\ I_{SC\_100\%\_T} &= I_{SC\_100\%\_0^o} + 0.00318 \cdot T. \end{aligned} \tag{14}$$

On the basis of (13) and (14), the PV cell model characteristics were implemented in Matlab software (Fig. 8).

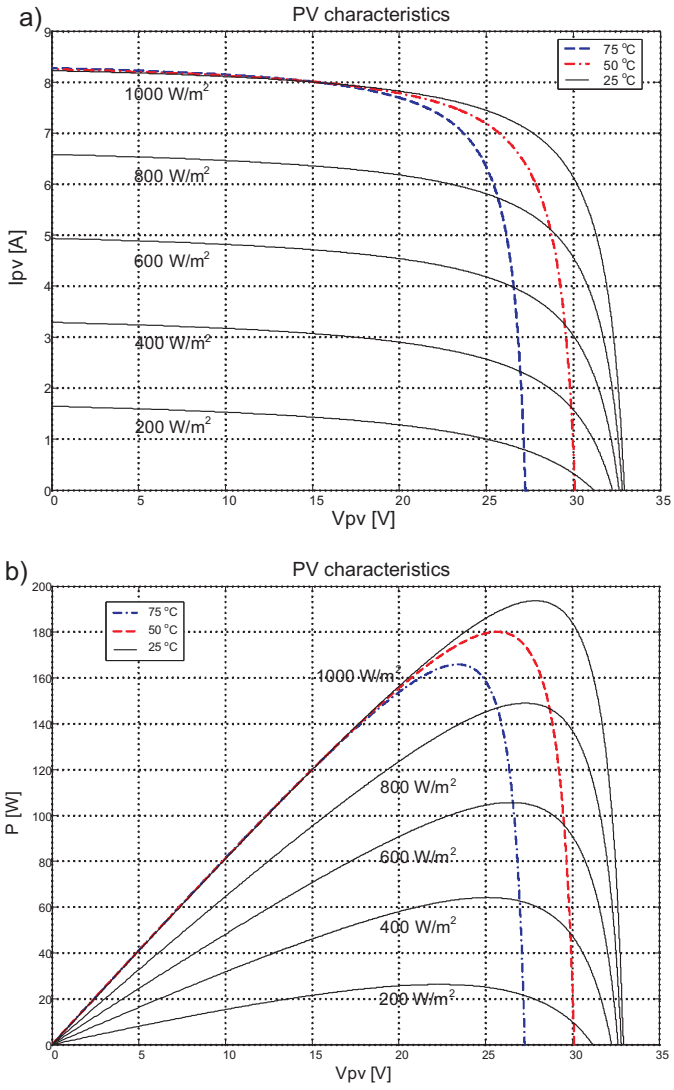

Fig. 8. PV cell model characteristics based on Kyocera KC200GT Cell after Ref. 6. Matlab software results: a) $I_{PV}(V_{PV})$, b) $P(V_{PV})$

Figure 9 presents the set of parameters and example results of FPGA-based model of PV panel, with simulated irradiation.

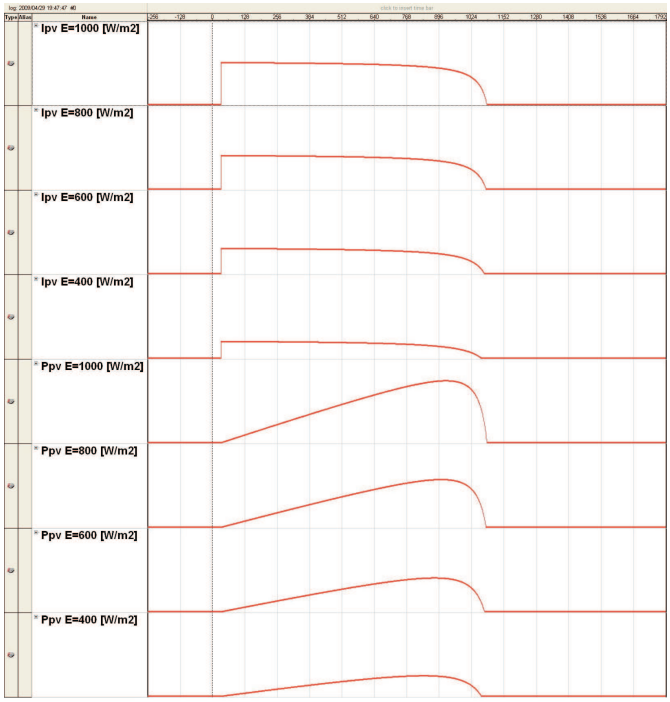

Fig. 9. Results of FPGA-based simulation of the PV cell model characteristic. Results from QuartusII/SignalTap Logic Analyzer software

3. The FPGA-based testing of single-phase grid connected systems

3.1. The single-phase grid-connected inverter. There are many topologies of power electronic converters applied in PV systems [2–3], e.g. multistring, AC-Modules, transformer or transformerless, with high frequency or low frequency transformer, with half-bridge or full-bridge inverter, with or without dc-dc stage, and many not typical cases [20]. The control strategy is also the field where many ideas are tested. Application of a full-bridge single-phase inverter enables control of unipolar or bipolar operation. The selection of a control method has a significant impact on filtering conditions of the grid current, dc current flow (in the input of the inverter), power losses on switches and common mode currents.

Figure 10 presents waveforms under bipolar and unipolar operations of the single phase grid-connected inverter. In the case of bipolar operation, the current that flows through dc input capacitor of the inverter has negative regions which can also increase losses (Fig. 10). The switching frequency component in the inverter output voltage under bipolar operation is two times higher than under unipolar operation, which makes the grid current more difficult for filtering in comparison to the unipolar operation case. The bipolar operation of the single phase inverter has the advantage of decreasing common mode currents generation [21].

$$v_{cm} = (v_{AO} + v_{BO})/2. \tag{15}$$

The value of common voltage in the case of bipolar operation in the single-phase inverter remains constant [21] (Fig. 10a).

a)

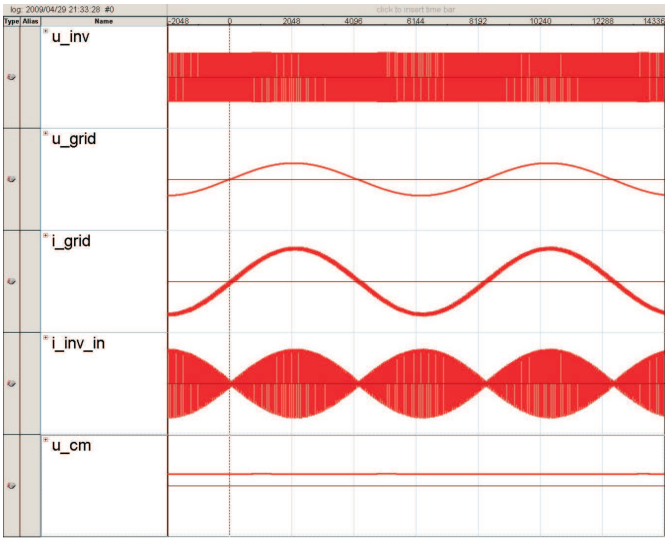

b)

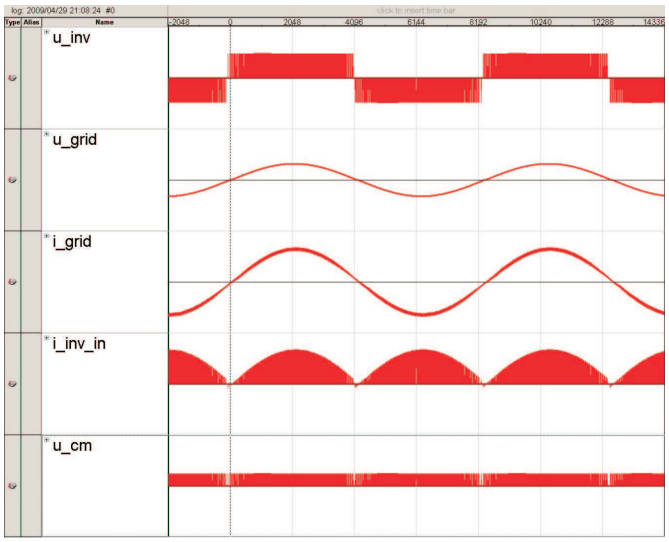

Fig. 10. Steady state operation of the single-phase grid-connected systems in case of bipolar and unipolar inverter operation with AC L (2 mH) filter, 18 kHz switching frequency: the grid voltage, the grid current, the inverter input current, common-mode voltage. Results of Quartus II/Signal Tap Logic Analyzer

For proper line current shaping, the inverter should be connected to the grid through an AC filter (Fig. 4, Fig. 11). The revision of ac filters can be found in [22] and [23]. The *LCL* AC filter enables greater dumping of the switching frequency component, from the L filter, in the generated current (Fig. 11).

Figure 12 presents waveforms (FPGA-based discrete simulations) that show impact of the AC filter topology on the grid current waveform in case of application L and *LCL* AC filter.

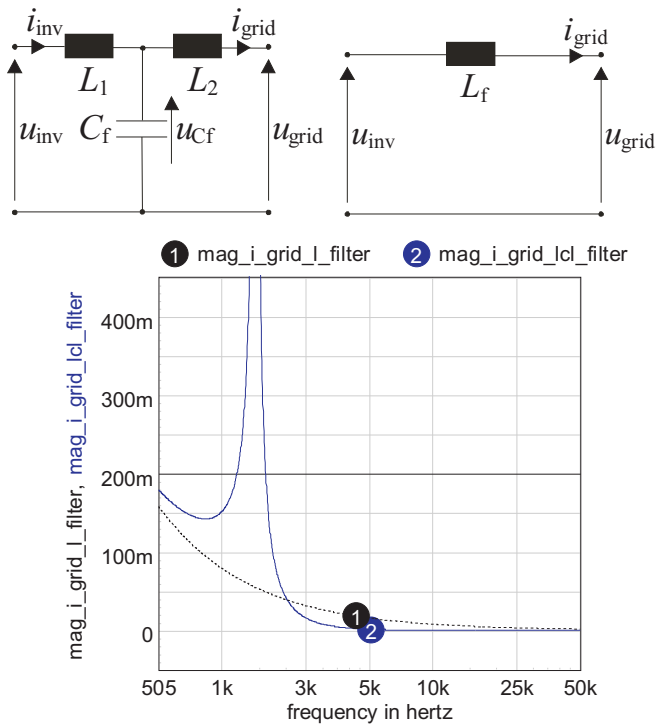

Fig. 11. Example of AC analysis results of L (2 mH) and LCL (2×750 μH, 25.5 μF) circuits (ICAP/4 Software AC analysis from inverter side)

For L filter (Fig. 11) the grid current calculation is realized by solving one (discrete) first-order differential equation:

$$L di_{\text{grid}}/dt + R \cdot i_{\text{grid}} = u_{\text{inv}} - u_{\text{grid}} \tag{16}$$

where $L = L_f + L_{\text{grid}}$; $R = R_f + R_{\text{grid}}$.

For LCL filter application it is necessary to solve the set of equations describing i_{inv}, i_{grid}, u_{Cf} [24]:

$$\begin{bmatrix} \frac{du_{\text{Cf}}}{dt} \\ \frac{di_{\text{inv}}}{dt} \\ \frac{di_{\text{grid}}}{dt} \end{bmatrix} = \begin{bmatrix} 0 & \frac{1}{C_f} & \frac{-1}{C_f} \\ \frac{-1}{L_1} & \frac{-R_1}{L_1} & 0 \\ \frac{1}{L_2} & 0 & \frac{-R_2}{L_2} \end{bmatrix} \begin{bmatrix} u_{\text{Cf}} \\ i_{\text{inv}} \\ i_{\text{grid}} \end{bmatrix} + \tag{17}$$

$$+ \begin{bmatrix} 0 \\ \frac{1}{L_1} \\ 0 \end{bmatrix} (u_{\text{inv}}) - \begin{bmatrix} 0 \\ 0 \\ \frac{1}{L_2} \end{bmatrix} u_{\text{grid}}.$$

The FPGA-based real-time modelling is a useful tool for different converters topologies verification. It enables testing steady state, failures and behavior of the system under special control (e.g. start of the converters). In this paper the control of the analyzed system is realized according to the conception presented in Fig. 4.

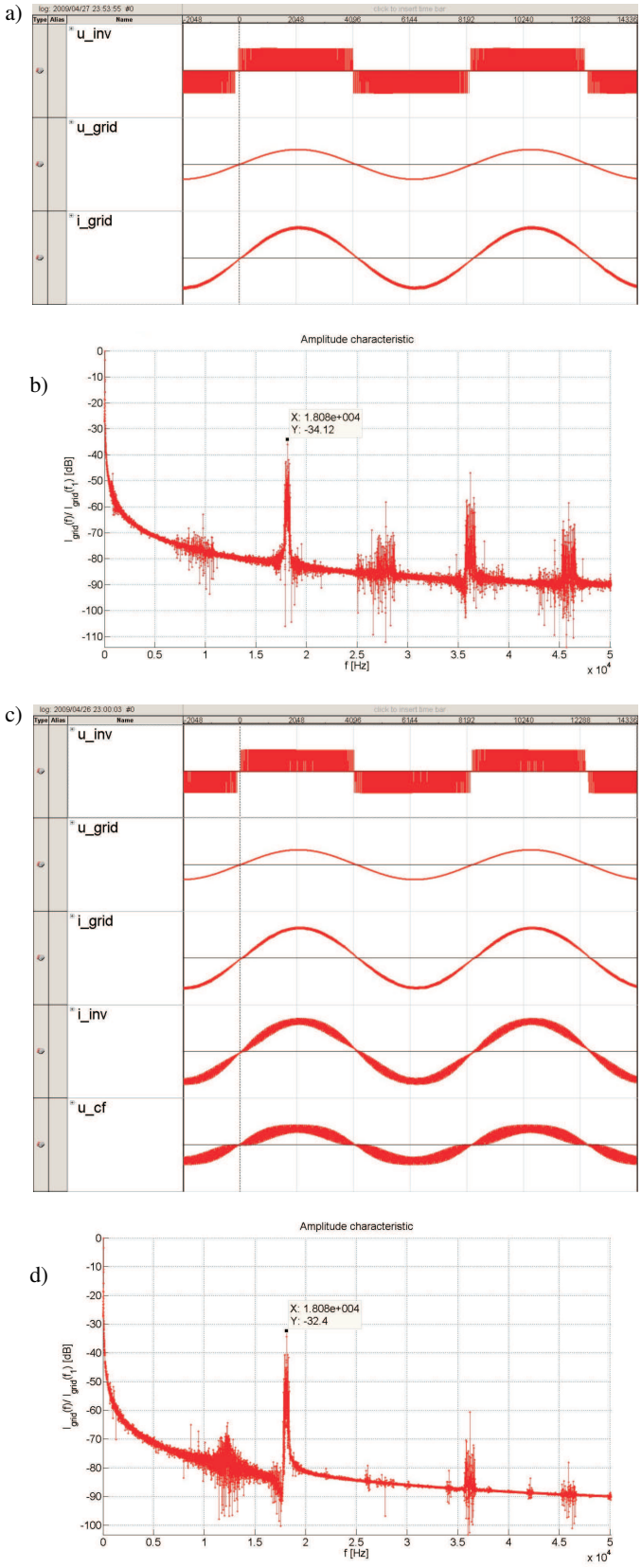

Fig. 12. Example of operation (QuartusII/SignalTap waveforms and the grid current amplitude characteristic calculated in MATLAB) of discrete model of the PV grid connected system with: a, b) L (2 mH), c, d) LCL (2×750 μH, 25.5 μF) AC filter

3.2. The inverter MPPT algorithm verification on the FPGA-based real-time model. The FPGA-based real-time model of the PV system can be a very functional tool for MPPT algorithms verification [17].

The MPPT algorithms search the conditions of system operation to obtain the maximum power from the PV system. The MPPT algorithms are mostly a modification of basic P&O (Perturb and Observe) technique [25]. In the tested model of PV system (Fig. 4a – the system without boost converter) a simple algorithm where MPPT unit analyses the PV source power and sets the amplitude of the reference current was tested (Fig. 13). The algorithm starts from the condition of slight current (start of the system) and goes to the maximum power in about 5 s.

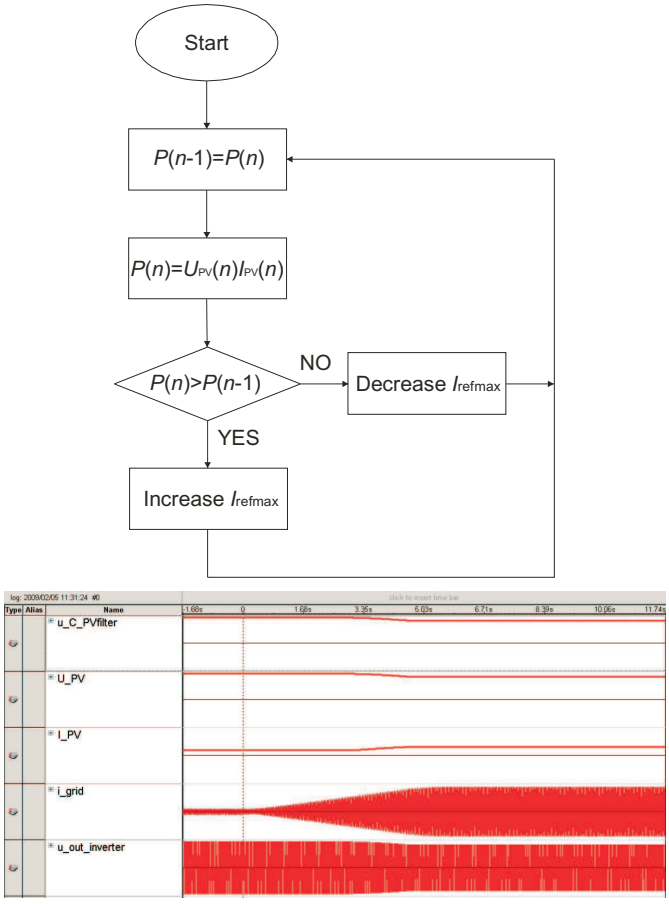

Fig. 13. Tested MPPT algorithm, and example of waveforms (start of the system) in the single-phase grid connected system with inverter connected directly to the PV source

In the single phase grid connected system the average power of the PV source may be decreased by 100 Hz variation of power on the output of the inverter. For efficient PV source exploitation a LC filter on the output of PV can be applied (especially in the case of the systems without boost converter). Figure 14 presents waveforms from the single-phase grid connected system with inverter connected directly to the PV source for two cases of the PV output filter. Application of the PV source output filter enables significant reduction of its 100 Hz power fluctuation.

a)

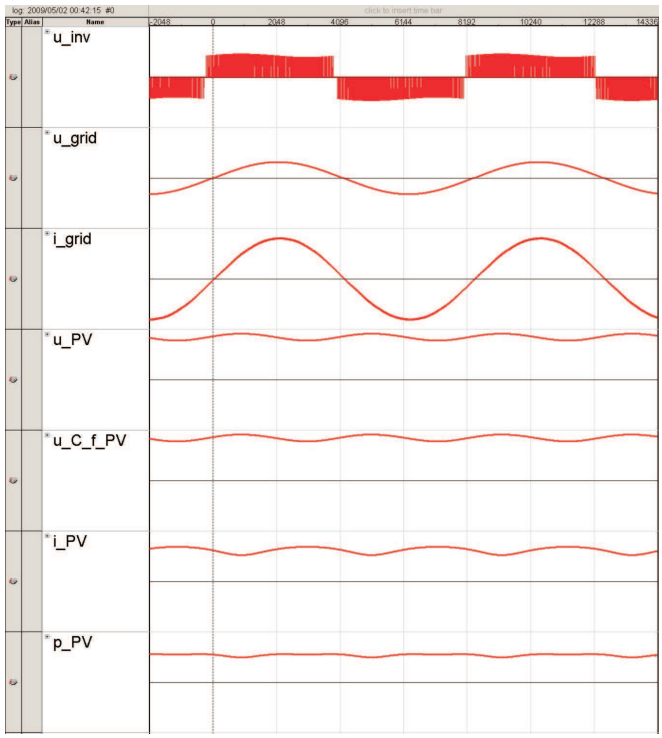

b)

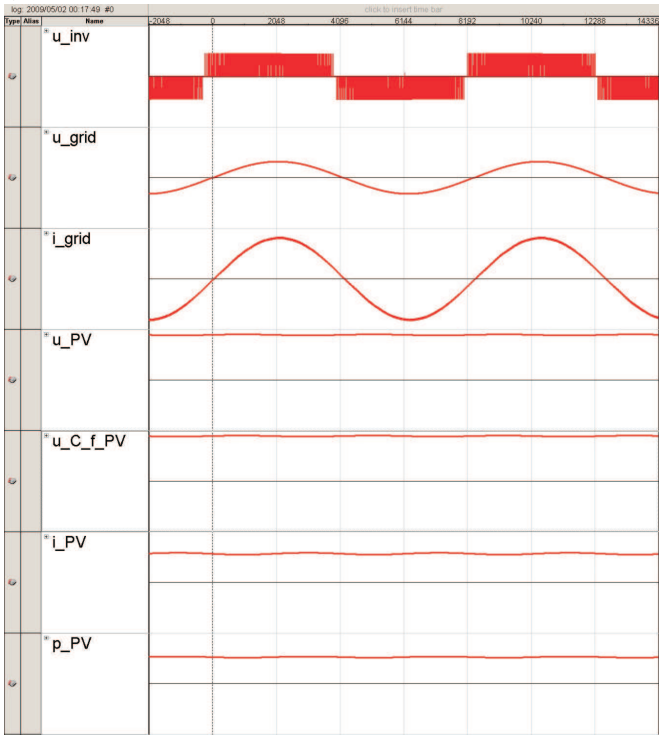

Fig. 14. Influence of the input filter parameters on the PV array current, voltage and power. Waveforms from the single-phase grid connected system with inverter connected directly to the PV source for the two cases of the PV output filter: $L_{fPV} = 0.25$ mH, $C_{fPV} = 1$ mF and $L_{fPV} = 0.25$ mH, $C_{fPV} = 6$ mF. Operation with 4kW power near MPP. 230 V/50 Hz single phase system. (Different scales used for waveforms, but the same settings in a and b case)

3.3. Boost dc-dc converter with PV source. In many topologies of PV systems (e.g. in grid-connected systems with low voltage PV panels) dc-dc converters are used. In most cases a boost converter (Fig. 15) is applied. Figure 16 presents FPGA-based real-time simulation waveforms of the boost DC/DC converter.

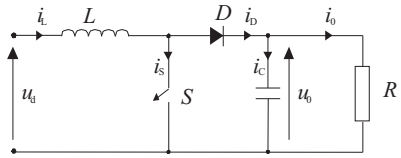

Fig. 15. Dc-dc boost converter

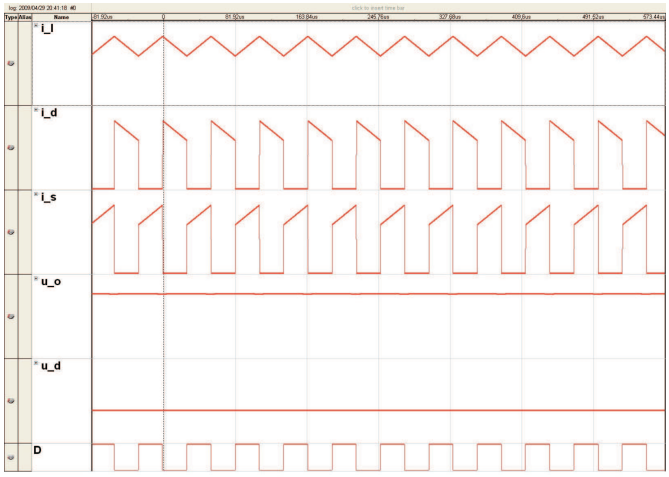

Fig. 16. Results of FPGA-based real-time simulation of boost converter in steady state: Inductor current i_l, diode current i_d, switch current i_s, output voltage u_o, input voltage u_d, control signal D. Component values: $C_{IN} = 120$ μF, $C_{OUT} = 120$ μF, $L = 720$ μH, $R = 350$ Ω. Boost converter operating frequency: $f = 18$ kHz, irradiance 1000 W/m^2, $T = 25°$C. Results from QuartusII/SignalTap Logic Analyzer software

Figure 17 presents modelled PV array and boost converter in closed-control loop. Figure 18 presents results of simulating boost converter response for reference voltage step variation (from 300 V to 400 V).

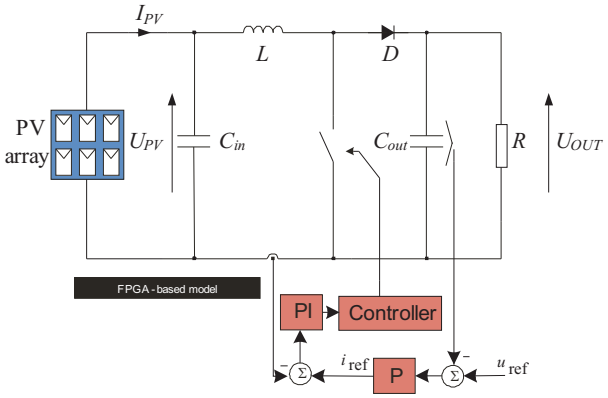

Fig. 17. PV array and boost converter in closed- control loop modeled in FPGA

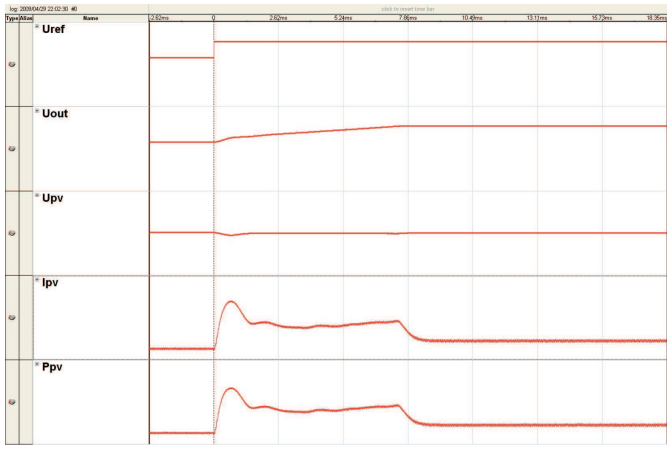

Fig. 18. Results of FPGA-based simulation of the dc-dc boost converter under closed-loop control system operation (dynamic state) – response on 300 to 400 V step of reference voltage level: U_{ref}, output voltage, PV voltage, PV current, PV power. Component values: $C_{IN} = 120$ μF, $C_{OUT} = 120$ μF, $L = 720$ μH, $R = 350$ Ω. Current controller: $K_P = 0.1$, $T_I = 5$ ms, Voltage controller: $K_P = 15$. Boost converter operating frequency: $f = 18$ kHz, irradiance 1000 W/m^2, $T = 25°$C. Results from QuartusII/SignalTap Logic Analyzer software

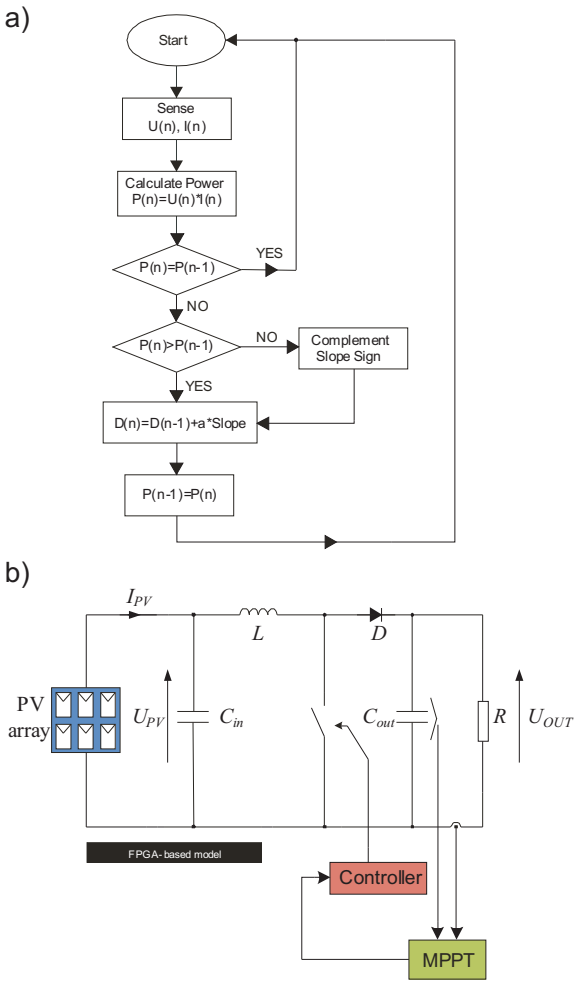

Fig. 19. HC MPPT technique: a) flowchart [25], b) application the MPPT in dc-dc boost converter

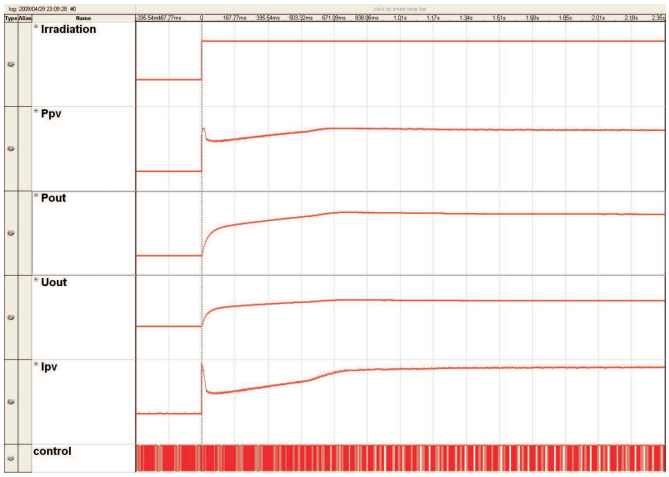

Fig. 20. Results of FPGA-based simulation of the dc-dc boost converter MPPT HC algorithm – response on irradiation 400 to 1000 W/m^2 step: Irradiation, PV power, Output power, Output voltage, PV voltage, PV current, control signal. Component values: $C_{IN} = 120$ μF, $C_{OUT} = 240$ μF, $L = 720$ μH, $R = 350$ Ω. MPPT controller: $a = 1.25 \cdot 10^{-3}$. Boost converter operating frequency: $f = 18$ kHz, $T = 25°$C. Results from QuartusII/SignalTap Logic Analyzer software. Maximal output power 1515.68 W

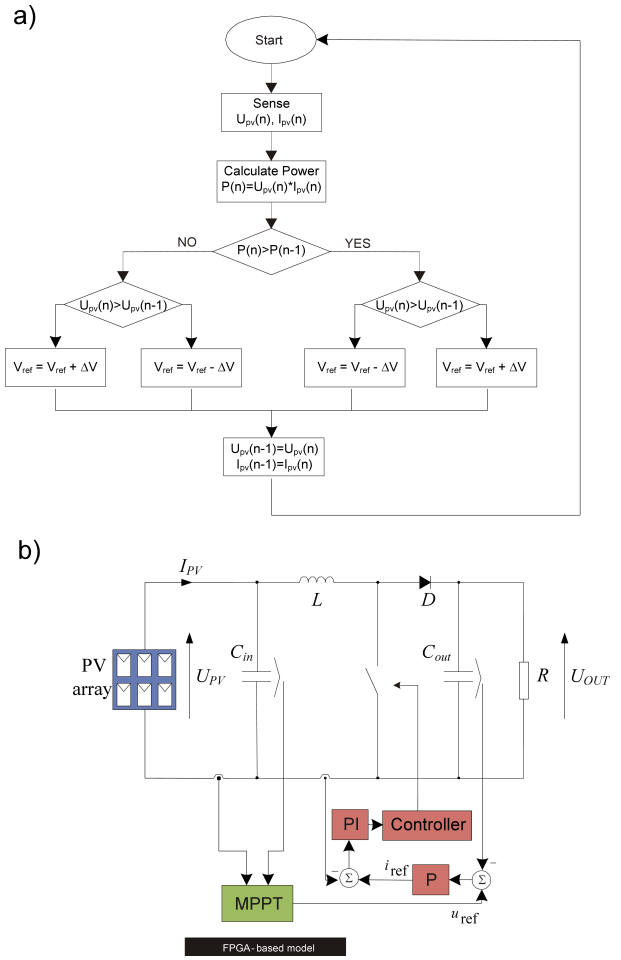

Fig. 21. P&O MPPT technique [25]: a) flowchart, b) dc-dc boost converter application

For testing the MPPT realisation by the boost converter, the models of converter with resistive load were used (Fig. 19b, Fig. 21b). There are many MPPT algorithms which provide this function [25]. One of the simplest is Hill Climbing algorithm (HC). This algorithm was implemented in the system presented in Fig. 19b. Figure 20 presents results of simulating boost converter response for irradiation change (HC algorithm) from 400 W/m^2 to 1000 W/m^2.

One of the most popular MPPT algorithms is Perturbation & Observation method (P&O) [25]. It bases on closed-control loop (Fig. 17) of dc-dc converter. Figure 21 presents P&O MPPT technique applicable in dc-dc converters [25].

4. Conclusions

In this paper the FPGA-based real-time simulation method for control verification of power electronic converters in grid-connected systems with energy generated from photovoltaic sources is proposed. The presented results, were obtained using FPGA-based models (PV source, power electronic converters, and filters) of power system, under FPGA-based control. This proves the usefulness of modelling the control circuit before its application in power system, which increases operational safety, reduces time-to-market and decreases costs of implementation. It also enables simulating many external condition cases which determine operation of the conversion system (e.g. irradiation or temperature of PV source, turning off the grid).

Acknowledgements. This work was supported by Ministry of Science and Higher Education in Poland as a research project No N N510389535.

REFERENCES

[1] M. Sibiński and Z. Lisik, "Polycrystalline CdTe solar cells on elastic substrates", *Bull. Pol. Ac.: Tech.* 55 (3), 287–292 (2007).

[2] J.M. Carrasco, L.G. Franquelo, J.T. Bialasiewicz, E. Galvan, R.C. Portillo Guisado, M.A.M. Prats, J.I. Leon, and N. Moreno-Alfonso, "Power-electronic systems for the grid integration of renewable energy sources: a survey", *IEEE Trans. on Ind. El.* 53 (4), CD-ROM (2006).

[3] F. Blaabjerg, F. Iov, R. Teodorescu, and Z. Chen, "Power electronics in renewable energy systems", *12th Int. Power Electronics and Motion Control Conf.* 1, CD-ROM (2006).

[4] D. Maliniak, *Basics of FPGAs Design*, *A Supplement to Electronic Design*, Mentor Graphics Corp., Wilsonville, 2003.

[5] *Cyclone III Device Handbook*, Vol. 1, Altera Corporation, New York, 2008.

[6] KC200GT, *KYOCERA*, datasheet (2001–2008).

[7] A. Parera Ruiz, M. Cirstea, W. Koczara, and R. Teodorescu, "A novel integrated renewable energy system modelling approach, allowing fast fpga controller prototyping", *11th Int. Conf. Optimization of Electrical and Electronic Equipment*, *OPTIM* 1, 395–400 (2008).

[8] R. Stala, "Testing of the grid-connected photovoltaic systems using FPGA-based real-time model", *13th Int. Power Electronics and Motion Control Conf.* 1, CD-ROM (2008).

[9] E. Koutroulis, K. Kalaitzakis, and V. Tzitzilonis, "Development of an FPGA-based system for real-time simulation of photo-

voltaic modules", *17th IEEE Int. Workshop on Rapid System Prototyping* 1, CD-ROM (2006).

[10] R. Ruelland, G. Gateau, T.A. Meynard, and J.M. Hapiot, "Design of FPGA-based emulator for series multicell converters using co-simulation tools", *IEEE Trans. on Power. Electron*. 18, 455–463 (2003).

[11] R. Stala, "Ac/ac multicell converter analysis on the basis of FPGA-based model of the converter", *Electrotechnical Review* 10, 28–36 (2007), (in Polish).

[12] C. Dufour, T. Ishikawa, S. Abourida, and J. Belanger, *Modern Hardware-in-the-Loop Simulation Technology for Fuel Cell Hybrid Electric Vehicles*, IEEE Publishing House, New York, 2007.

[13] M.N. Cirstea and A. Dinu, "A VHDL holistic modeling approach and FPGA implementation of a digital sensorless induction motor control scheme", *IEEE Trans. on Ind. Electron.* 54 (4), CD- ROM (2007).

[14] C. Dufour, S. Abourida, and J. Belanger, "Real-time simulation of permanent magnet motor drive on FPGA chip for high-bandwidth controller tests and validation", *IEEE ISIE* 1, CD-ROM (2006).

[15] L.A.C. Lopes and A.M. Lienhardt, "A simplified nonlinear power source for simulating PV panels", 34^{th} *IEEE Power Electronics Specialist Conf.* 4, 1729–1734 (2003).

[16] P.T. Krein, "Tricks of the trade: a simple solar cell model", *IEEE Power Electronics Society Newsletter* 1, CD-ROM (2001).

[17] M.A. Vitorino, L.V. Hartmann, A.M.N. Lima, and M.B.R. Corrêa, "Using the model of the solar cell for determining the maximum power point of photovoltaic systems", *12th Eur. Conf. Power Electronics and Applications* 1, CD-ROM (2007).

[18] O.M. Midtgard, "A simple photovoltaic simulator for testing of power electronics", *12th Eur. Conf. Power Electronics and Applications* 1, CD-ROM (2007).

[19] U. Böke, "A simple model of photovoltaic module electric characteristics", *12th Eur. Conf. on Power Electronics and Applications* 1, CD-ROM (2007).

[20] Y. Jiang, Z. Chen, J. Pan, X.I. Zhao, and P. Lee, "A novel phase-shift full-bridge converter with voltage-doubler and decoupling integrated magnetics in PV system", *Bull. Pol. Ac.: Tech.* 56 (3), 285–293 (2008).

[21] R. González, J. López, P. Sanchis, E. Gubía, A. Ursúa, and L. Marroyo, "High-efficiency transformerless single-phase photovoltaic inverter", *EPE-PEMC* 1, CD-ROM (2006).

[22] S. Vasconcelos Araújo, A. Engler, B. Sahan, F. Luiz, and M. Antunes, "LCL filter design for grid-connected NPC inverters in offshore wind turbines", *7th Int. Conf. Power Electronics* 1, CD-ROM (2007).

[23] M. Raou and M.T. Lamchich, "Average current mode control of a voltage source inverter connected to the grid: application to different filter cells", *J. Electrical Engineering* 55 (3–4), 77–82 (2004).

[24] K. Masoud and G. Ledwich, "Grid connection via third order filter: near-deadbeat control", *AUPEC* 1, CD-ROM (2000).

[25] M.C. Cavalcanti, K.C. Oliveira, G.M. Azevedo, D. Moreira, and F.A.Neves, "Maximum power point tracking techniques for photovoltaic systems", *Electrotechnical Review* 2, 49–56 (2006).